Journal of Power Sources 231 (2013) 163–172

Contents lists available at SciVerse ScienceDirect

Journal of Power Sources

journal homepage: www.elsevier.com/locate/jpowsour

Carbon monoxide and methanol oxidations on Pt/X@MoO_3/C (X = Mo_2C, MoO_2, Mo^0) electrodes at different temperatures

O. Guillén-Villafuerte [a], G. García [a,b,*], R. Guil-López [b], E. Nieto [b], J.L. Rodríguez [a], J.L.G. Fierro [b], E. Pastor [a,**]

[a] Departamento de Química Física, Instituto Universitario de Materiales y Nanotecnología, Universidad de La Laguna, Avda. Astrofísico Francisco Sánchez s/n, La Laguna, 38071 Tenerife, Spain
[b] Grupo de Energía y Química Sostenibles (EQS), Instituto de Catálisis y Petroleoquímica, CSIC, C/Marie Curie 2, Cantoblanco, 28049 Madrid, Spain

HIGHLIGHTS

- Core–shell Mo-particles were tested as Pt catalyst support.
- CO and methanol oxidation reactions were studied in the 20–70 °C temperature range.
- Core–shell Mo-particles act only as promoter for these reactions.
- CO and methanol oxidation is enhanced by facile OH formation and electronic effects.

ARTICLE INFO

Article history:
Received 5 October 2012
Received in revised form
17 December 2012
Accepted 27 December 2012
Available online 5 January 2013

Keywords:
Carbon monoxide oxidation
Methanol oxidation
Fuel cell
Molybdenum carbide
Catalyst support
Temperature

ABSTRACT

The present study is focused in the use of *core–shell* molybdenum substrates as supports for Pt electrocatalysts. These substrates are prepared by the carbothermal-reduction method and present a *core–shell* structure, with a reduced-Mo *core* (Mo_2C, MoO_2 and/or Mo^0) and a MoO_3 *shell*. Kinetic and mechanistic studies were performed through potentiodynamic and potentiostatic experiments for carbon monoxide and methanol oxidation reactions on Pt/X@MoO_3/C (X = Mo_2C, MoO_2, Mo^0) catalysts in an intermediate temperature range ($20 < T < 70$ °C). Results reveal the promoter effect and the great stability of Mo-carbide based substrates for both reactions in the temperature range studied. Carbon monoxide and methanol oxidation on Pt/X@MoO_3/C are enhanced by a facile oxygenated species formation, better dispersion of the active phase and electronic effects. It is concluded that the best catalyst performance during the methanol oxidation reaction was obtained with the substrate that contains only Mo_2C-phase in its core.

1. Introduction

Polymer electrolyte fuel cells (PEMFCs) are one of the most promising devices for both portable and stationary applications due to its high power density at low work temperatures (55–95 °C), low weight, compactness and suitability for discontinuous operation [1–4]. Principal problems associated to PEMFCs are hydrogen storage; carbon monoxide traces in the fuel (if the fuel is obtained from reforming processes), high cost catalysts and the loose of catalytic component due to highly corrosive medium [1–5].

On the other hand, if an organic molecule is used as fuel (e.g. methanol), no-previous reforming processes are required and it can be directly supplied at the anode of a fuel cell (FC). Additionally, if the organic molecule is liquid at ambient temperature, the distribution and market of this type of technology could be easier (e.g. it could be used in the petrol network). In this sense, direct methanol fuel cell (DMFC) appears as a very promising technology. However, some drawbacks need to be solved before attaining an effective marketing. More representative problems in a DMFC are [1–4,6–8]: i) mix-potential at the cathode due to methanol crossover; ii) incomplete fuel oxidation that decreases the energy conversion efficiency; iii) surface reaction intermediate formation that acts as catalytic poison (e.g. CO_{ad}); iii) poor electrode kinetics at the anode and cathode; and iv) high catalyst cost and the loose of catalytic component due to highly corrosive media.

* Corresponding author. Grupo de Energía y Química Sostenibles, Instituto de Catálisis y Petroleoquímica, Consejo Superior de Investigaciones CSIC, C/Marie Curie 2, Cantoblanco, 28049 Madrid, Spain. Tel.: +34 915854947; fax: +34 915854760.
** Corresponding author. Dpto. de Química Física, Instituto de Materiales y Nanotecnología, Universidad de La Laguna, C/Astrofísico Francisco Sánchez s/n, 38071 La Laguna, Spain. Tel.: +34 922318071; fax: +34 922318010.
E-mail addresses: gonzalo@icp.csic.es (G. García), epastor@ull.es (E. Pastor).

0378-7753/$ – see front matter © 2013 Elsevier B.V. All rights reserved.
http://dx.doi.org/10.1016/j.jpowsour.2012.12.099

Concerning methanol oxidation on Pt-based electrodes in acidic media, much effort was done during last decades. For a detailed discussion, the reader is referred to several literature reviews [1,9–12]. As summary, the mechanism for methanol oxidation involves two main steps:

i) Electrosorption and dehydrogenation of methanol onto the substrate: methanol needs a suitable surface for its adsorption and the subsequent dehydrogenation steps. In this sense, it is well known that at least three neighbouring Pt atoms are necessary to fully complete the dehydrogenation steps yielding adsorbed carbon monoxide (CO_{ad}) [12]. In addition to CO_{ad}, several intermediates and by-side products such as formaldehyde and formic acid can be formed [7,8,13]. Recently, Cuesta et al. showed the importance of the ensemble effect during the methanol dehydrogenation on Pt(111) surface modified with cyanide adatoms [14]. They demonstrated that methanol could be fully oxidized to carbon dioxide, avoiding the principal catalytic poisoning (CO_{ad}), when only two contiguous Pt atoms are present onto the surface. It is noticeable that this step becomes important at low (ambient) temperatures [1,6].
ii) Electrooxidation of CO_{ad}: addition of oxygenated species (O or OH from water) to CO_{ad} to form CO_2 is needed, and consequently the catalytic surface is liberated. There is a large body of work of current agreement that the electrooxidation of CO_{ad} follows the Langmuir–Hinshelwood mechanism, which was first proposed by Gilman [15]. In this mechanism, first the oxygenated species are formed on the surface trough a charge transfer reaction. After that, a chemical reaction between both adsorbed species (CO_{ad} and OH_{ad}) is produced, and finally, an electrochemical reaction occurs to generate CO_2.

Assuming this general mechanism and processes, a lot of effort has been done in order to produce catalysts with an enhanced ability to remove CO from the catalytic surface. In this sense, different strategies to improve catalysts activity are normally used, being the electronic effect and bi-functional mechanism the most accepted mechanisms involved in the modification of metal properties [1,5,6]. The first one is related to alter the electronic structure of the catalyst (e.g. Pt) by alloying with another metal (e.g. Ru) and/or by varying densities and structures of the atomic surface (introducing atomic defects such as kink, step, border, etc). On the other hand, the bi-functional mechanism is associated to easier water dissociation (oxygenated species formation) due to the addition (alloying is not necessary) of an oxophilic system into the catalyst. In this context, the foreign system can also catalyse the reaction or be just a promoter (co-catalyst).

Actually, Pt–Ru alloys, with a Pt to Ru atomic ratio of 1:1, display the highest catalytic activity towards methanol oxidation [1,6,7,11,16,17]. In fact, most of the studies were performed using carbon (Vulcan, nanotubes, etc.) as supports for this type of catalyst [6,11,16,18], and the enhanced activity towards methanol oxidation was ascribed to both effects, i.e. electronic and bi-functional. However, these supported catalysts present a lack in their stability along the time in highly corrosive environment in DMFCs.

In this context, carbides appear as good candidates to be employed as support for FC electrocatalysts. Their higher resistance towards corrosion and degradation under FC working conditions make this type of material unequivocally attractive to be used as catalyst support in the fuel cell field [19–21]. Furthermore, recent studies using transition and/or rare earth metal oxides as catalyst support suggest better dispersion of the active phase (e.g. Pt) in association with a promotional effect. The latter was related to the modification of the electronic state of the active phase by the catalyst support [22]. In this sense, we have recently demonstrated that Mo-core@MoO_3-shell particles with different Mo phases in their core (Mo_2C, MoO_2 and a mix of Mo_2C, MoO_2 and Mo^0) used as Pt support, have higher stability and catalytic activity towards CO and CH_3OH oxidation than the corresponding Pt catalyst supported on a Vulcan carbon (C) [21]. The Pt/Mo_2C@MoO_3/C catalyst, with a single crystalline Mo_2C phase inside presents the best catalytic activity and stability. Catalyst supports with the presence of Mo oxide phases (MoO_2) showed higher activity, but their stability was not good enough. Furthermore, we proved that X@MoO_3 particles act not only as promoter for CO removal from Pt, but also for methanol oxidation [21].

Despite Pt/X@MoO_3/C being a good catalyst, there is still lacking of kinetic and mechanistic studies for CO and methanol oxidation on these systems. The present paper focuses on understanding the kinetics and mechanisms of these reactions on diverse Pt/X@MoO_3/C. Thus, core–shell Mo-particles, with a reduced-Mo core (Mo_2C, MoO_2 and/or Mo^0) and a MoO_3-shell, were prepared and used as support for Pt nanoparticles to investigate in detail the CO and methanol oxidation at different temperatures in acidic media.

2. Experimental

2.1. Electrocatalysts synthesis

Catalysts have been prepared using a synthesis method described in our earlier work [21]. Briefly, the electrocatalysts preparation is divided into three stages: (i) incorporation of Mo-precursor [$(NH_4)_2MoO_4 \cdot 4H_2O$, Sigma–Aldrich] to the carbon black Vulcan support (C, XC-72, Cabot) by modification of the standard wet impregnation method; (ii) carburization of Mo-precursor by the carbothermal reduction method and subsequent surface passivation in order to stabilize the highly reactive reduced Mo-phase/s, obtaining core–shell particles with a reduced Mo-phase(s) in the core and MoO_3 in the surface that are supported on C (X@MoO_3/C; X = Mo_2C, MoO_2, Mo^0); and (iii) finally, X@MoO_3/C samples were treated by the wet impregnation method with an appropriate amount of 8 wt% H_2PtCl_6 solution (Sigma–Aldrich), in order to obtain 20 wt% Pt/X@MoO_3/C catalysts. After the impregnation step, Pt nanoparticles were obtained following the formic acid reduction method (FAM) [23].

After the Mo-salt impregnation, the carburization process of the Mo-salt/C sample was performed by the carbothermal reduction method, using H_2 (10 vol% H_2/Ar at 100 mL min^{-1}) as reducing agent and the C-support as carbon source. Different carburization conditions (temperature, time, etc) were tested in order to obtain materials with several Mo-phases on C surface and materials with only one Mo-phase/C. In this way, the control of the carburization conditions was used to prepare samples with different Mo-phases: one with several Mo-phases (MoO_2, Mo_2C, Mo^0) and other two with one reduced Mo-phase, Mo_2C or MoO_2, respectively. After the carburization, the pyrophoric reduced Mo-samples were stabilized by passivation with pulses of 5 vol% O_2/He. Consequently, a MoO_3 surface into the Mo-particles was produced. These three reduced molybdenum samples are denoted in the text with the corresponding Mo-phase (Table 1) [21].

Additionally, for comparative purposes, a Mo-free Pt supported on C electrocatalyst was prepared (20 wt% Pt) following the same procedure described above.

2.2. Electrocatalysts characterization

Briefly, Mo-content was determined by thermogravimetry through the loss of weight during carbon support combustion under a flow of air (100 mL min^{-1}) using a Mettler Toledo TGA/SDTA 851

Table 1
Nomenclature and Mo phase composition inside the core of the Pt/X@MoO_3/C catalysts.

Catalyst	Pt/C	Pt/Mo_2C@MoO_3/C	Pt/MoO_2@MoO_3/C	Pt/Mo_{mix}@MoO_3/C
Mo phase in the core	–	Mo_2C	MoO_2	$Mo_2C + MoO_2 + Mo^0$

thermal analyser and checked by ICP-chemical analysis (plasma analysis). Pt-loadings of the Pt/X@MoO_3/C and Pt/C-reference electrocatalysts were obtained by energy dispersive X-ray analysis (EDX), coupled to the scanning electron microscopy (SEM) LEO Mod. 440 equipment. Powder XRD patterns of Pt/X@MoO_3/C catalysts were recorded in a Seifert XRD 3000P diffractometer, using Cu-K_α radiation ($\lambda = 1.54050$ Å) and AT Diffract software, with a scanning rate of 0.04° s^{-1}. Crystalline phases were identified by comparing the experimental diffraction patterns with the Joint Committee on Powder Diffraction Standards (JCPDS) [24]. The XPS spectra were acquired with a VG Escalab 200R spectrometer equipped with a hemispherical electron analyzer and an MgK_α ($h\nu = 1253.6$ eV) X-ray source. The constant charging of the samples was corrected by referencing all energies to the C1s peak at 284.6 eV. Pt-particle sizes were evaluated from TEM images recorded in a JEOL 2100F microscope operated with an accelerating voltage of 200 kV and equipped with a field emission electron gun providing a point resolution of 0.19 nm, and checked by XRD technique using the Scherrer equation with the (220) characteristic peak of Pt ($2\theta = 70°$) of the Pt/X@MoO_3/C sample patterns. The Pt/X@MoO_3/C catalysts patterns were obtained with a Carl Zeiss-Jena, URD-6 diffractometer, under the same conditions. Physicochemical characterization of synthesized materials was recently described in detail in Refs. [20,21].

2.3. Electrocatalytic studies

Cyclic voltammetry (CV) and chronoamperometry techniques were used to determine the catalytic activity of the Pt/X@MoO_3/C catalysts towards the oxidation of carbon monoxide (CO, Air Liquide, 99.997%) and methanol (MeOH, Merck p.a.). Electrochemical measurements were carried out in a standard three-electrode electrochemical cell in $20 \leq T \leq 70$ °C temperature range with an Autolab PGSTAT302 (Ecochemie) potentiostat. The working electrodes consist of 20 μL of catalyst ink (4 mg ml^{-1} of catalyst) deposited onto a glassy carbon electrode of 5 mm in diameter. A carbon rod was used as counter electrode and a reversible hydrogen electrode (RHE) in the supporting electrolyte was employed as reference electrode. All potentials in the text are referred to this electrode. First to any experiment, the working electrode was immersed in the electrolyte solution and the potential was cycled several times between 0.05 and 0.90 V vs RHE at a scan rate of 0.2 V s^{-1} ("activation step") until a reproducible voltammogram was obtained in the base electrolyte (0.5 M H_2SO_4). All solutions were prepared using ultrapure water (Millipore Milli-Q system).

2.3.1. Electrooxidation of CO_{ads}

The CO tolerance of the Pt/X@MoO_3/C electrocatalysts and the reference Pt/C one was characterized by CO_{ads} stripping experiments in 0.5 M H_2SO_4 solution performed at different temperatures. CO was bubbled for 10 min at 0.07 V vs. RHE and subsequently argon for 30 min (Ar, Air Liquide, 99.999%) was used to degas the solution during 30 min. After that, the potential was scanned from the adsorption potential down to 0.05 V (so the hydrogen adsorption region can be checked) and then up to 0.90 V, and three consecutive cycles were recorded at 0.02 V s^{-1}. First cycle corresponds to the CO_{ads} electrooxidation, while the second and third cycles show the background voltammogram, indicating that all adsorbed carbon monoxide was removed from the catalyst. Electrochemical active areas (electroactive areas) were determined from the integration of the current involved in the oxidation of a CO monolayer taking into account that CO adsorbs only on Pt (recently we demonstrated that CO does not adsorb on X@MoO_3/C substrates [21]). All calculated current densities were normalized with respect to this electroactive area.

2.3.2. Methanol electrooxidation

Catalytic activity of the Pt/X@MoO_3/C catalysts towards MeOH electrooxidation in 0.5 M H_2SO_4 solution was characterized by CV and chronoamperometry techniques. The catalyst was immersed at the controlled potential of 0.05 V into the working solution. After that, the CV was scanned from 0.05 up to 0.90 V at a scan rate of 0.02 V s^{-1} and four consecutive cycles were recorded. Current transients were performed at 0.65 V in 1 M CH_3OH + 0.5 M H_2SO_4 solution in order to evaluate the performance along the time of the electrocatalysts for MeOH oxidation. Experiments were carried out in a wide temperature range ($20 \leq T \leq 70$ °C), and current was normalized with respect to the electroactive area.

3. Results

3.1. CO stripping

Fig. 1 shows the CO stripping voltammograms of Pt/C performed at all the temperatures investigated. Typical CO stripping curves are observed with a main CO oxidation peak at potentials more positive than 0.6 V proceeded by an anodic shoulder. The anodic shoulder

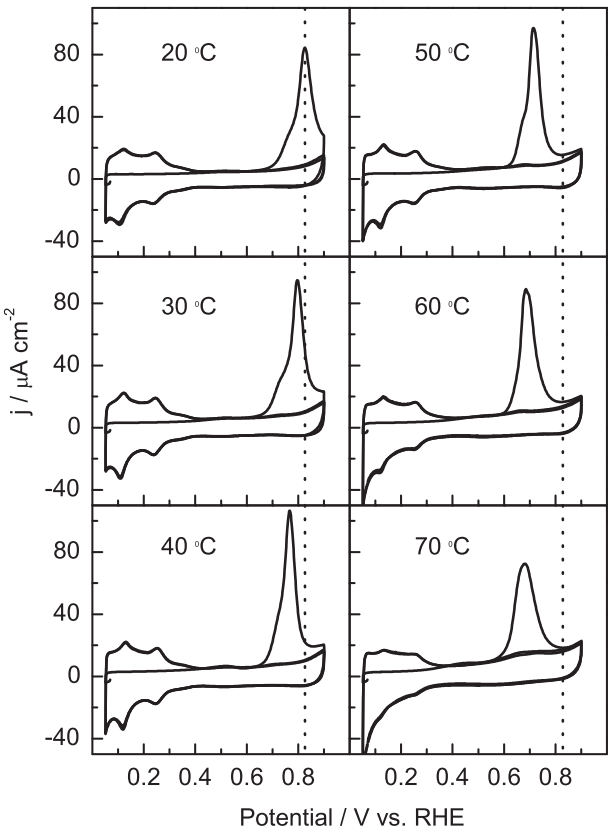

Fig. 1. CO stripping on Pt/C catalyst in 0.5 M H_2SO_4. $\nu = 20$ mV s^{-1}.

and the main peak are associated to the CO oxidation at sites with different activities [5,25]. Accordingly, the small charge under the anodic shoulder has to be related to a low density of the highest active sites. Also, it can be seen that the shape of the main anodic CO oxidation currents was significantly modified with the temperature, accompanied with a negative shift of the peak oxidation potential. For example, for the CO stripping recorded at 20 °C the main oxidation peak is located at 0.82 V presenting a shoulder at 0.77 V, while for the same experiment performed at 60 °C the shoulder disappears and the main CO oxidation peak becomes symmetric at 0.76 V. In the same way, the onset potential shifts to more negative potentials with increasing the temperature. The present results corroborate that CO oxidation and diffusion towards the most active catalytic site are thermally activated in the temperature range of this study.

Figs. 2–4 show the CO stripping experiments performed between 20 and 70 °C for the three Pt/X@MoO_3/C catalysts. First of all, there are clear differences between these catalysts and the Pt/C counterpart (Fig. 1) during the CO stripping and subsequent voltammograms. The main difference in the base electrolyte is the quasi-reversible contribution at ca. 0.45 V, which does not depend on the temperature or Mo phases in the support. These peaks were ascribed to Mo^{+4}/Mo^{+6} redox couple formed at the passivation step during the synthesis of the support, which is the same for all the samples [21], i.e. all the Mo-based catalysts have the same shell (MoO_3) but different cores.

On the other hand, a new anodic peak at ca. 0.4 V is observed for all Pt/X@MoO_3/C catalysts during the CO stripping experiments. In fact, recently we confirmed by differential electrochemical mass spectrometry (DEMS) that this anodic peak involves the CO and Mo oxidation reactions [21]. Remarkably, the onset potential for CO oxidation reaction is close to 0.1 V. Additionally it is visible that all Pt/X@MoO_3/C catalysts present similar features during the CO oxidation reaction: two broad anodic contributions (peaks) at ca. 0.4 and 0.7 V. The broad CO oxidation peak developed at higher potentials is formed by several anodic peaks, which depend of the Mo phase inside the core. Summarizing, different catalytic sites are present onto the Pt/X@MoO_3/C surface, i.e. highly active sites at very negative potentials and other active sites at more positive

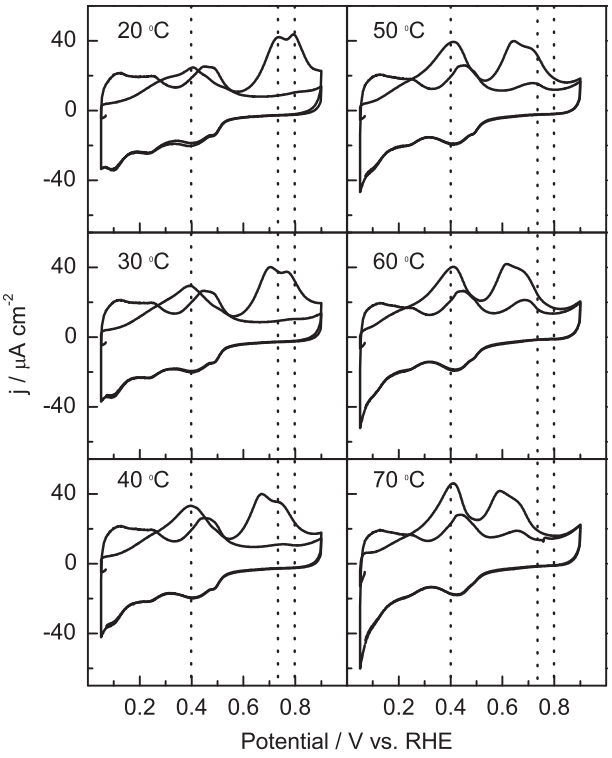

Fig. 3. CO stripping on Pt/MoO_2@MoO_3/C catalyst in 0.5 M H_2SO_4. ν = 20 mV s^{-1}.

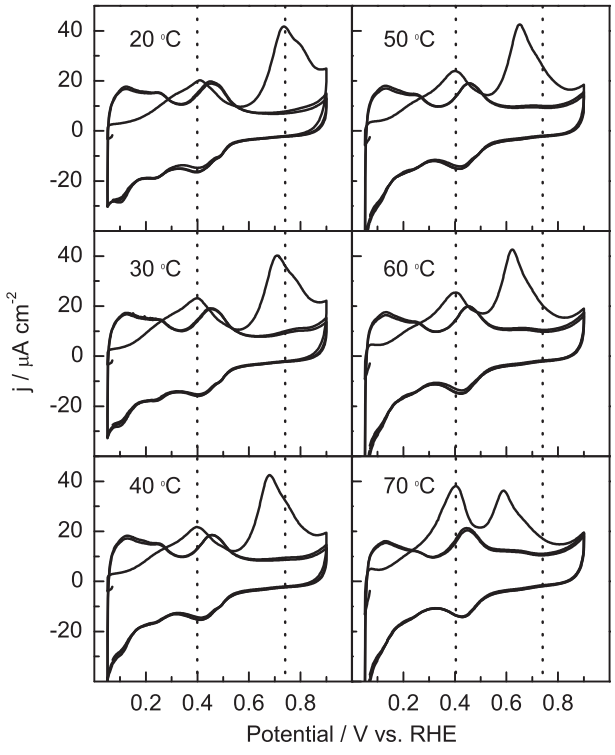

Fig. 2. CO stripping on Pt/Mo_{mix}@MoO_3/C catalyst in 0.5 M H_2SO_4. ν = 20 mV s^{-1}.

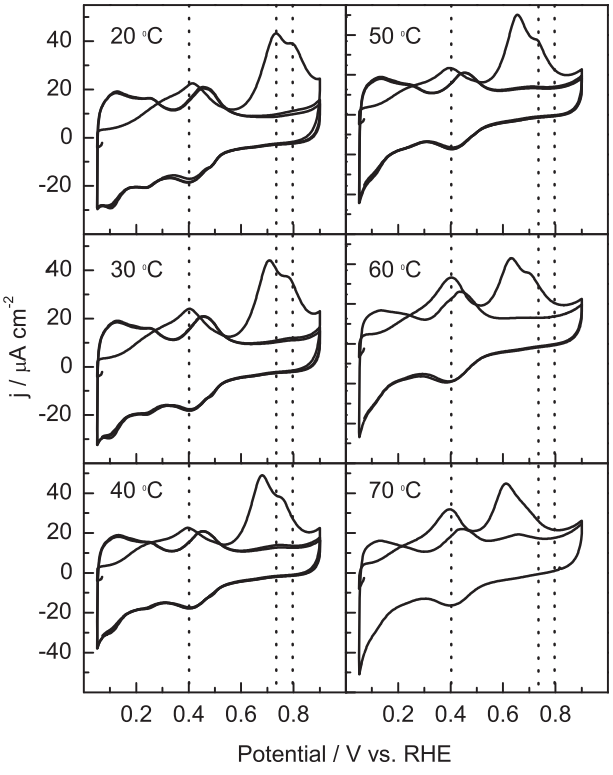

Fig. 4. CO stripping on Pt/Mo_2C@MoO_3/C catalyst in 0.5 M H_2SO_4. ν = 20 mV s^{-1}.

potentials, the relative quantity of the two types of sites depends on the nature of Mo phase into the core of the support particles.

It is noticeable that both broad anodic peaks are developed at more negative potentials (0.4 and 0.7 V) when X@MoO_3/C is used as catalyst support. In this sense, it is well known the positive effect of transition and rare metal oxides on Pt-group metals during the CO oxidation reaction [22]. The increase in the catalytic activity was ascribed to the development of electron enriched Pt sites by a direct electronic effect promoted by the interaction of the noble metal and the transition and/or rare metal oxides [22]. Similar effect may work with the catalyst support used in the present manuscript.

On the other hand, the electrooxidation charge involved in the anodic peaks at low and high potentials increases and decreases, respectively as temperature rises. This fact clearly suggests a link between both catalytic sites, i.e. CO that is firstly adsorbed on all active sites, diffuses fast on the surface from the least to the most active sites with the increment of the temperature. Even more intriguing is that the peak potential of the contribution at ca. 0.4 V remains constant with the temperature. On the other hand, the broad peak potential at ca. 0.7 V shifts to more negative potentials with the increase of temperature reproducing the trend observed before for Pt/C catalyst. Nevertheless, the onset and peak potentials for the contribution around 0.7 V appear considerably at more negative potentials when X@MoO_3/C samples are used as support.

3.2. Methanol oxidation

Fig. 5 shows the first two cyclic voltammograms during the methanol oxidation on Pt/C in acidic media recorded at 0.02 V s^{-1} within the 20–70 °C temperature range. It is remarkably that the working electrode was introduced into the cell at controlled potential of 0.05 V. Therefore, a competitive adsorption between hydrogen and methanol is expected. It is clearly observed the typical increase of the current density and the negative shift of the onset potentials as the temperature rise.

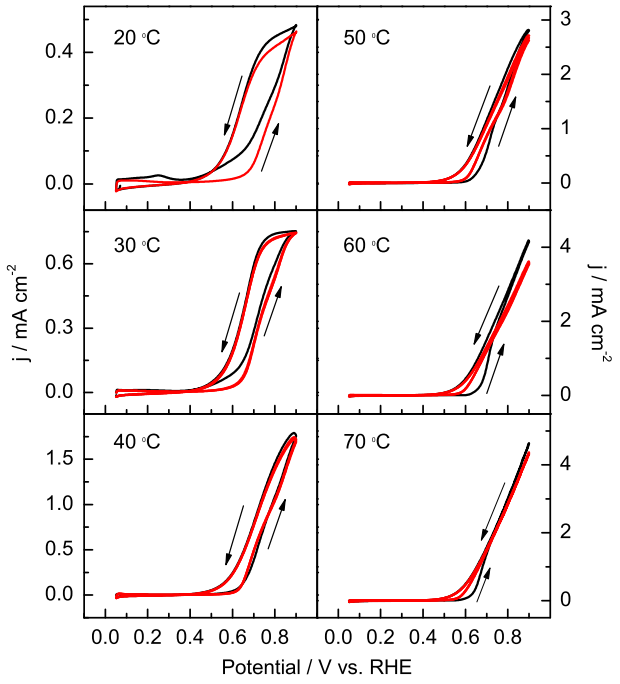

Fig. 5. Voltammetric profiles for the Pt/C catalyst in 1 M methanol + 0.5 M H_2SO_4 solution (1st and 2nd cycles are black and red, respectively). ν = 20 mV s^{-1}. (For interpretation of the references to colour in this figure legend, the reader is referred to the web version of this article.)

A close view of the first anodic scan is displayed in Fig. 6. In this figure, two potential regions can be distinguished which account for the two main steps of methanol oxidation reaction. The electrosorption and dehydrogenation step occur at $E < 0.4$ V and it is very important at temperatures below 40 °C. The electro-oxidation of methanolic fragments, such as CO_{ad}, is apparent at $E > 0.4$ V and it becomes the most important step at temperatures above 40 °C. Actually, the anodic current developed at $E < 0.4$ V at 20 and 30 °C is related mostly to the hydrogen desorption reaction, which competes significantly with methanol adsorption (note the anodic current diminution with the increment of the temperature). On the other hand, at temperatures higher than 40 °C, methanol adsorption and dehydrogenation steps become facile in this potential range [1,6], and consequently, the active sites become fast poisoned by methanolic fragments (mainly CO_{ad}). Thus, CO_{ad} coverage at $E < 0.4$ V increases in the subsequent way: 20 < 30 < 40 < 50 < 60 °C. Nonetheless, CO_{ad} coverage decreases at 70 °C, which is associated to a weakening of the CO adsorption strength [26].

In this context, CO_{ad} coverage has a great importance in the methanol oxidation reaction. It is evident that at 60 °C (highest CO_{ad} coverage in the present conditions), the onset potential for methanol oxidation is at ca. 0.6 V, which is the same value observed for the onset potential during the oxidation of a CO_{ad} monolayer on Pt/C (Fig. 1). Therefore, it can be concluded that all catalytic sites are blocked by CO_{ad} at 60 °C and methanol can react only after the electrooxidation step (CO removal) which occurs at $E > 0.6$ V. Finally, methanol electrooxidation becomes faster at $E > 0.6$ V. Thus, the electro-oxidation step governs the kinetics in the subsequent CVs and the onset potential for methanol oxidation becomes similar ($\approx$0.6 V) for all the temperature range studied.

Figs. 7–9 show the methanol oxidation on Pt/X@MoO_3/C catalysts at all temperatures studied in the present work. Firstly, similar onset potential is established for methanol oxidation at all Pt/X@MoO_3/C catalysts during the first three CVs. The latter suggests an improvement of the electrosorption and dehydrogenation step compared with the Pt/C catalyst, which could be associated to

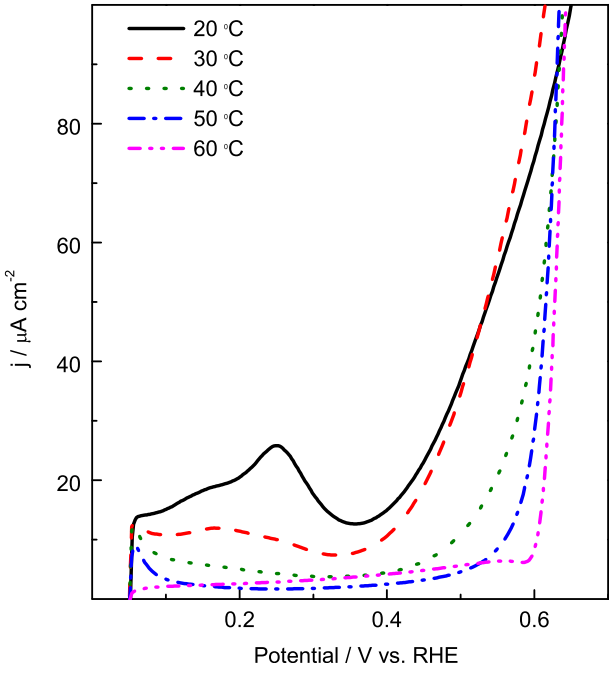

Fig. 6. Zoom of the voltammetric profiles during the first cycle for the Pt/C catalyst in 1 M methanol + 0.5 M H_2SO_4 solution. ν = 20 mV s^{-1}.

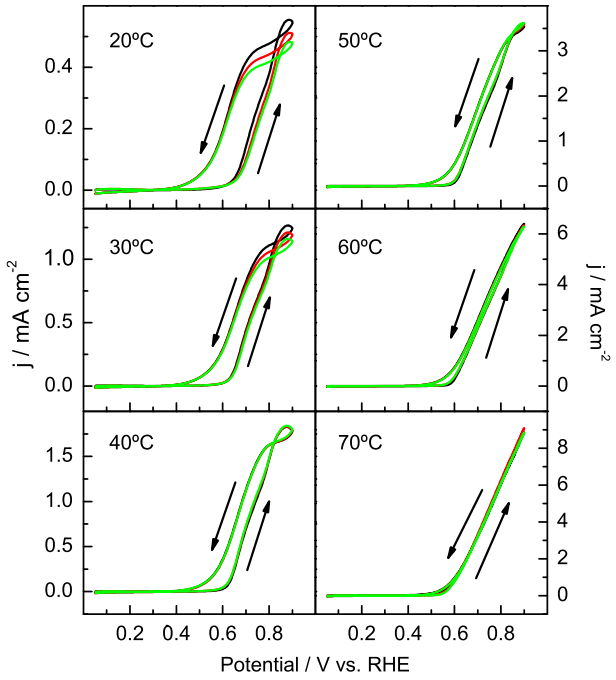

Fig. 7. Voltammetric profiles for the $Pt/Mo_{mix}@MoO_3/C$ catalyst in 1 M methanol + 0.5 M H_2SO_4 solution (1st, 2nd and 3rd cycles are black, red and green, respectively). $\nu = 20$ mV s^{-1}. (For interpretation of the references to colour in this figure legend, the reader is referred to the web version of this article.)

a better dispersion of the noble metal on Mo-based supports. However, analysing in detail these figures, small differences can be detected between the first and second CVs in the onset potential for methanol oxidation on $Pt/MoO_2@MoO_3/C$ and $Pt/Mo_{mix}@MoO_3/C$ catalysts at 20 °C. Thus, $Pt/Mo_2C@MoO_3/C$ appears as the more suitable catalyst for methanol adsorption and dehydrogenation step.

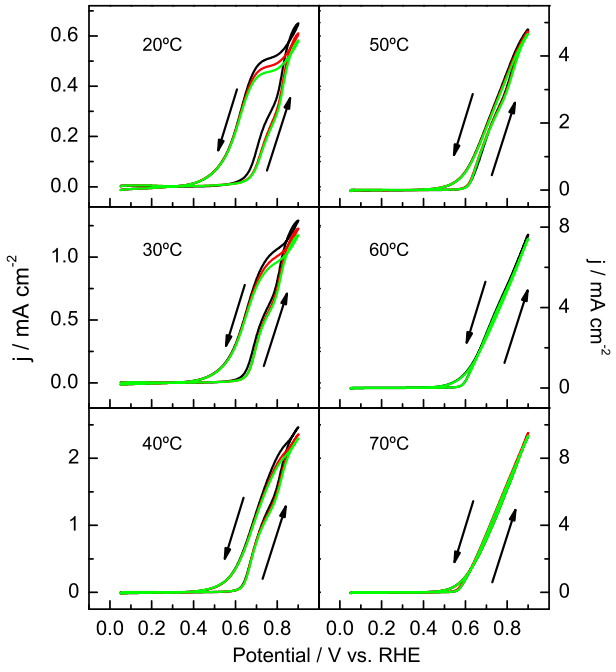

Fig. 8. Voltammetric profiles for the $Pt/MoO_2@MoO_3/C$ catalyst in 1 M methanol + 0.5 M H_2SO_4 solution (1st, 2nd and 3rd cycles are black, red and green, respectively). $\nu = 20$ mV s^{-1}. (For interpretation of the references to colour in this figure legend, the reader is referred to the web version of this article.)

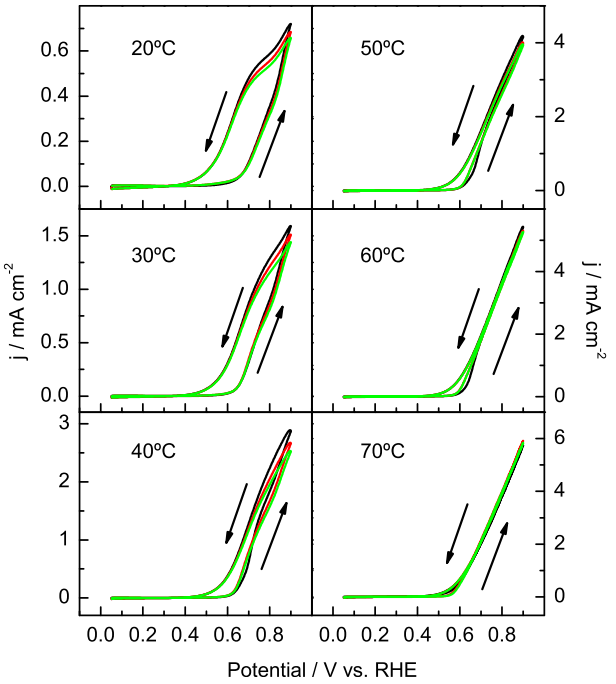

Fig. 9. Voltammetric profiles for the $Pt/Mo_2C@MoO_3/C$ catalyst in 1 M methanol + 0.5 M H_2SO_4 solution (1st, 2nd and 3rd cycles are black, red and green, respectively). $\nu = 20$ mV s^{-1}. (For interpretation of the references to colour in this figure legend, the reader is referred to the web version of this article.)

On the other hand, all $Pt/X@MoO_3/C$ catalysts develop higher anodic currents than Pt/C counterpart during the methanol oxidation reaction in all temperature range studied. Again, better dispersion of the Pt nanoparticles and the electronic effect produced by the Mo-based support appear as responsible for the enhanced activity [22]. However, the maximum current density during the methanol oxidation on $Pt/X@MoO_3/C$ catalysts drops continuously during the subsequent CVs at temperatures below 40 °C, indicating a low but visible poisoning of the active sites. It is noticeable that the methanol oxidation rate depends on the core nature of the $X/MoO_3/C$ support. $Pt/MoO_2@MoO_3/C$ presents higher maximum current density than $Pt/Mo_{mix}@MoO_3/C$ in all temperature range, while $Pt/Mo_2C@MoO_3/C$ catalyst develops the highest and lowest values at low ($T \leq 40$ °C) and high ($T \geq 60$ °C) temperatures, respectively.

Finally, current transients were recorded during the methanol oxidation on all catalysts at 0.65 V in the previously mentioned temperature range. At this stage is important to remark that DMFCs work typically at 0.4–0.5 V [3,4]. However, in the present communication Pt-based catalysts are tested without addition of a second precious metal such as Ru, and a more positive potential has to be selected to obtain detectable currents. Actually, we are just proving the importance of the catalyst support in FC systems.

Chronoamperometric curves were studied with the purpose to compare the current densities under potentiostatic conditions, which are more representative for FC studies than the previous potentiodynamic curves displayed in Figs. 5–9. Fig. 10 shows the current densities decay along the time at 0.65 V. It is observable that the methanol oxidation rate is different for each catalyst at each temperature. Additionally, it is evident that in all cases the use of $X@MoO_3/C$ support improves considerably the methanol oxidation at short times, but their performance depends on the core nature, which is in perfect agreement with previous potentiodynamic experiments (Figs. 5–9). For example, $Pt/MoO_2@MoO_3/C$ catalyst develops the highest oxidation current at short times, but falls very

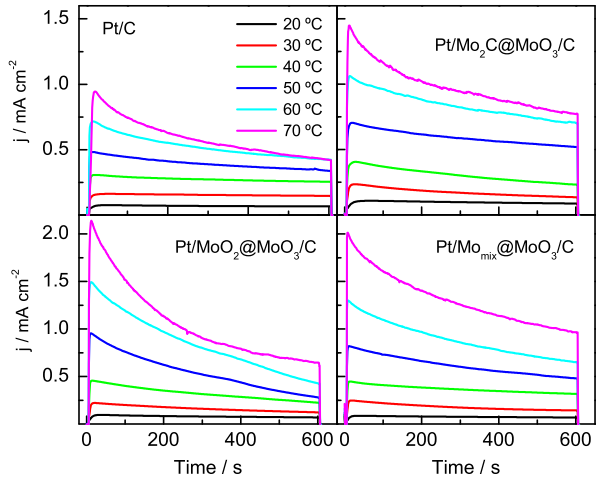

Fig. 10. Current transients measured at different temperatures (20, 30, 40 50, 60, 70 °C), recorded at 0.65 V vs. RHE for Pt/C and Pt/X@MoO_3/C catalysts in 1 M methanol + 0.5 M H_2SO_4 solution.

fast, which is indicative of a loss in the catalytic activity. Comparing the different catalysts, it can be established that the highest stability of the steady current was recorded during methanol oxidation on Pt/Mo_2C@MoO_3/C. The latter is in agreement with previous works in which long stability was achieved using transition and/or rare earth metal oxides as support [22].

Arrhenius plots (ln(current) vs $1/T$) are given in Fig. 11 for all catalysts. Apparent activation energies (E_{ap}) were obtained from these plots. Two different slopes with a visible break at 40 °C were found for all catalyst. The E_{ap} values for Pt/C, Pt/Mo_2C@MO_3/C, Pt/Mo_{mix}@MO_3/C and Pt/MoO_2@MO_3/C were 51/10, 38/19, 58/33, and 45/38 kJ mol^{-1} in the temperature range between $20 \leq T \leq 40$ °C and $40 \leq T \leq 70$ °C. Indeed, the curve of Pt/MoO_2@MO_3/C is more like a straight line with a slope close to 37 kJ mol^{-1}. Interestingly, similar temperature value (40 °C) was obtained during the voltammetric study (Figs. 5 and 6) for a drastic onset potential change during the methanol oxidation reaction. Additionally, the developed current densities have a clear dependence with the nature of the catalyst support.

4. Discussion

4.1. CO stripping

The asymmetry and/or existence of more than one peak during the CO stripping on Pt/C may be associated to the presence of sites

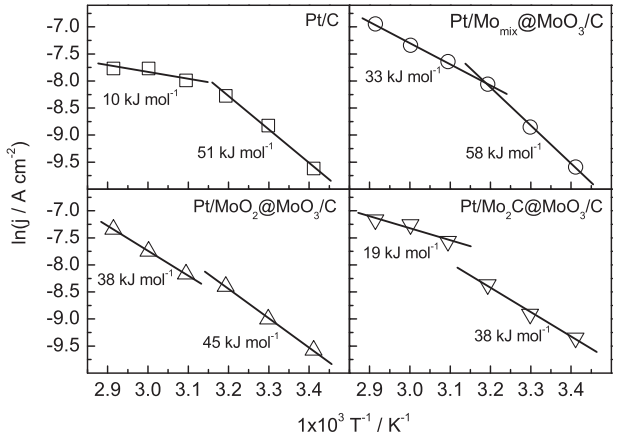

Fig. 11. Arrhenius plot at 0.65 V vs. RHE for Pt/C and Pt/X@MoO_3/C catalysts.

with different catalytic reactivity and geometry on the Pt nanoparticle surface [5,27,28]. Recently, Gisbert et al. [27] studied the CO oxidation reaction on poly-oriented and single-crystal Pt electrodes in phosphate solution for a wide pH range. They found a correlation between the diverse CO oxidation peaks on Pt poly-oriented electrode with those of the Pt basal planes. Moreover, several studies using Pt nanoparticles with well-defined surface structure have shown the same correlation [28], i.e. it is possible to prepare nanoparticles presenting different surfaces with diverse atomic array that corresponds manly to a specific basal plane.

On the other hand, Lebedeva et al. [29–31] studied the CO oxidation in acidic media on Pt stepped single-crystals, which present terraces with (111) and steps with (110) orientations. They demonstrated that the CO_{ad} diffusion on the terrace is very fast and that the CO oxidation occurs mainly on the Pt(110) steps (the most reactive site in their conditions).

According to these results, we suggest that Pt/C nanoparticles prepared in this work are mainly formed by surfaces with different atomic geometry of quite long order and that the density of low coordinated sites (kink, steps, edges, etc.) is very low. Consequently the CO oxidation occurs at very positive potentials. The shift to more negative potentials of CO oxidation with the temperature can be explained by the increase of CO diffusion and the enhancement of water dissociation. In this way, CO can diffuse and reacts onto the most active site, and accordingly, only one symmetric peak is developed at high temperatures (Fig. 1).

On the other hand, literature describes in some detail that the addition of a second metal to the base catalyst can produce an enhancement of the CO oxidation reaction due to electronic effects and/or bi-functional mechanism [1,11]. Moreover, it is well known that the use of transition metal oxides as catalyst support is beneficial for CO removal [22]. Recently, we demonstrated that X@MoO_3/C does not adsorb CO [21]. Also, it was observed a very poor catalytic activity towards the electro-oxidation of dissolved CO and methanol [21]. In the present paper, it is shown that when an active metal, such as Pt, is supported on X@MoO_3/C, the catalytic activity towards adsorbed CO oxidation is considerably enhanced compared with Pt/C (Figs. 1–4). Therefore, we can state that X@MoO_3/C acts only as promoter (co-catalyst) during the CO oxidation reaction.

Additionally, similar features are observed, during CO oxidation at the different Pt/X@MoO_3/C catalysts. Therefore, it is reasonably to ascribe the enhancement in the CO oxidation reaction to the MoO_3 shell, which is the same for all catalysts. Assuming the absence of alloying between Pt and X@MoO_3/C from XRD studies, the increment of the CO oxidation rate can be explained by a bifunctional mechanism, i.e. X@MoO_3/C provides oxygenated species at lower potentials than Pt. However, an additional tentative explanation for this effect involves electronic considerations, i.e. the development of electron enriched Pt sites by electronic transfer from the transition metal oxide to the noble metal. Therefore, the binding of CO at Pt/C is electronically different from the binding of CO at Pt/X@MoO_3/C, because the "local" Pt site potential is more negative when Mo-based support is used, and consequently, an increased back donation occurs. Accordingly, it is to be expected that this difference in the binding energy to the surface must somehow be reflected in the kinetics of CO oxidation.

Singular is the difference between both main CO oxidation peaks at Pt/X@MoO_3/C catalysts. Their differences may be explained considering Pt particles placed in different environments:

i) Respect to the potential peaks developed at higher potentials (broad anodic peak), they shift in a typical way with the increase of the temperature (Figs. 2–4). However, CO oxidation reaction is enhanced by the use of X@MoO_3/C support.

This result can be explained by an easier oxygenated species (OH_{ads}) production regarding the support, which is improved with the rise of the temperature. Also, electronic effect could be considered as responsible for this effect, since the binding energy of OH_{ads} may vary with the "local" potential. Additionally, CO diffusion is increased with the temperature and reacts faster on the most active sites. So, the onset and peak potentials shift towards more negative values as the temperature increases.

ii) Concerning the oxidation of the CO peak developed at lower potentials, the charge involved increases with the temperature. It is relevant to stress that this increment is associated with the charge diminution of the anodic peak at higher potentials. Therefore, there is a link between both main active sites, i.e. anodic peaks developed at 0.4 and 0.7 V. On the other hand, the peak centred at 0.4 V does not shift with the temperature. Thus, it is concluded that in the temperature range considered, adsorbed oxygenated species production is not affected as these species are formed very fast onto the X@MoO_3/C support in the present conditions.

4.2. Methanol oxidation

As described before, the mechanism for methanol oxidation involves two main steps: i), electrosorption and dehydrogenation, and ii), electrooxidation. The first step can be described as follows:

$$CH_3OH \rightarrow CH_3OH_{ad} \quad (1)$$

$$CH_3OH_{ad} \rightarrow CH_2O + 2H^+ + 2e^- \quad (2)$$

$$CH_3OH_{ad} + H_2O \rightarrow HCOOH + 4H^+ + 4e^- \quad (3)$$

$$CH_3OH_{ad} \rightarrow CO_{ad} + 4H^+ + 4e^- \quad (4)$$

First, adsorption of methanol needs a suitable surface (1). Afterwards, diverse dehydrogenation reactions may happen depending on the whole system conditions (2–4). For example, on an active surface that contains three or more contiguous Pt-atoms [14], formaldehyde can be formed and flow to the bulk solution or readsorbs to form acetic acid or carbon monoxide [7,8].

Following the same idea, formic acid can be formed from methanol (3) and/or formaldehyde, and it can diffuse to the bulk solution or further oxidized to carbon dioxide. In this context, if the diffusion path of soluble species (e.g. formaldehyde and formic acid) through the electrode is obstructed, the conversion efficiency towards CO_2 will be increased [7,8], i.e. the readsorption process is favoured.

However, the CO_{ad} formation, which is the principal catalyst poison, decreases the catalytic activity (rate) towards methanol oxidation. In this sense, Cuesta [14] proved that active surfaces with only two Pt neighbours produce CO_2 avoiding the CO path. Nevertheless, this is not our case and at the moment seems to be difficult to produce practical fuel cell electrodes with these conditions.

Finally, in our experiments, CO_{ad} may produce carbon dioxide through the electro-oxidation step in the following way [15]:

$$H_2O \rightarrow OH_{ad} + H^+ + e^- \quad (5)$$

$$CO_{ad} + OH_{ad} \rightarrow COOH_{ad} \quad (6)$$

$$COOH_{ad} \rightarrow CO_2 + H^+ + e^- \quad (7)$$

From these equations become clear the importance of the presence of oxygenated species for the enhancement of CO_{ad} removal.

Arrhenius plots can be used to estimate the operating mechanism for methanol electrooxidation. In this sense, the dependence of E_{ap} for Pt/C with the temperature reflects the change in the reaction mechanism, i.e. in the rds (rate determining step): the electrosorption and dehydrogenation step can be considered as the rds at $T < 40$ °C while the electro-oxidation step as the rds at $T > 40$ °C. The latter is in agreement with the methanol electrooxidation curves recorded during the first cycle of the potentiodynamic experiments (Figs. 5 and 6), in which the onset potential has a marked positive shift at temperature above 40 °C.

The observed adsorption competence between hydrogen and methanol at temperatures lower than 40 °C (Fig. 6) reinforce the stated before. Additionally, the higher current density delivered at temperatures below 40 °C and potentials lower than 0.6 V indicate that CO_{ad} is not (fast) produced (CO_{ad} oxidation occurs at potentials higher than 0.6 V). Therefore, it is reasonably to consider the by-side products formation at temperatures below 40 °C [8]. Afterwards, the rate of CO_{ad} production increases at potentials higher than 0.6 V and, as a consequence, the active sites become poisoned and the faradaic current is inhibited during the subsequent cycles. Thus, onset potential for methanol oxidation becomes equal during the subsequent CVs.

On the other hand, the electrosorption and dehydrogenation step (CO_{ad} formation) for Pt/C turns out to be facile at temperatures above 40 °C and, as consequence, the methanol oxidation rate turns to be governed by the electro-oxidation step [1,6]. Hence, the first and the subsequent CVs during the methanol oxidation reaction on Pt/C present similar onset potential (Fig. 5) at 40 °C. However, as the temperature increases (higher than 40 °C), the onset potential for methanol oxidation reaction during the first cycle is higher than in subsequent voltammograms. This result is due to the higher CO production at higher temperatures that completely blocks the active surface (in this context, it should be recalled that the working electrode was introduced at controlled potential of 0.05 V). So, the applied potential should be sufficiently positive to remove the CO_{ad}. Afterwards, during the subsequent voltammogram the onset potential shifts towards more negative potentials because the active surface is not fully blocked at the present sweep rate (0.02 V s^{-1}) and methanol can reacts on free catalytic sites. Similar behaviour is observed in the potentiostatic study (Fig. 10), in which the fast current decay at temperatures above 40 °C has to be associated to a rapid active surface poisoning by CO_{ad}. These results are in agreement with those obtained from Arrhenius plots, in which E_{ap} at temperatures higher than 40 °C is five times lower than E_{ap} obtained at lower temperatures, i.e. an external mass transfer limitation is happening clearly at this electrode [32].

Regarding to Pt/X@MoO_3/C catalysts, their onset potential during methanol oxidation is similar for all catalyst at the first and subsequent cycles in the temperature range investigated (Figs. 7–9). However, inspection of these figures reveals that the developed current densities as well as its decay along the cycles depend on the catalyst. Moreover, the current transient behaviour is characteristic of each support (Fig. 10). Therefore it is concluded that X@MoO_3/C supports participate in the methanol oxidation reaction depending of the nature of Mo phase(s) in the core. Considering the use of core–shell Mo-particles, with a reduced-Mo core (Mo_2C, MoO_2 and/or Mo_{mix}) and equal MoO_3-shell, differences have to be related with the nature of the core and therefore electronic effects must be invoked to understand the present results.

It is observed that current densities decay with time (Fig. 10), especially when Mo-containing particles are used as support. Thus, catalyst deactivation can arise from diverse factors such as oxidation of the surface and blockage of the catalytic sites by adsorbed organic residues (i.e. CO_{ad}) [1,4,9,11]. The last case seems not to be the reason for the faster deactivation of Pt/X@MoO_3/C

catalyst respect to Pt/C one, as enhanced catalytic activity for methanol electrooxidation at 0.6 V towards CO_{ad} oxidation reaction are established when X@MoO_3/C are used as catalyst supports (Figs. 2–4). In fact, it was observed a link between both main active sites (anodic peaks at 0.4 and 0.7 V) for CO oxidation reaction on Pt/X@MoO_3/C, in which the CO diffusion from the least to the most active site is temperature and time dependent.

Concerning the chronoamperometric curves for Pt/X@MoO_3/C catalysts at 0.65 V (Fig. 10), the highest anodic currents at short times, but also the highest current decays along the time, are achieved with Pt/MoO_2@MoO_3/C and Pt/Mo_{mix}@MoO_3/C catalysts, while Pt/Mo_2C@MoO_3/C one appears as the most stable material (similar current decay to Pt/C catalyst is recorded but higher stationary current values are archived). In this sense, it is well known that metal oxides, such as Pt or Ru oxides, are not active for methanol oxidation [8–11]. In this situation, methanol adsorption is not favoured, and consequently, the oxidation reaction rate decays. A possible explanation for the deactivation observed in Fig. 10 can be based on the presence of non-completed reduced species at the core of MoO_2@MoO_3/C and Mo_{mix}@MoO_3/C supports.

Summarizing, catalysts with MoO_2 in their core (Pt/MoO_2@-MoO_3/C and Pt/Mo_{mix}@MoO_3/C) produce high catalytic activity towards methanol oxidation at short times but are rapidly deactivated, whereas Pt/Mo_2C@MoO_3/C catalyst, with only Mo_2C phase in its core, generates enhanced and stable steady currents along the time.

Arrhenius plots are in agreement with the suggested above (Fig. 11). Similar E_{ap} is obtained for all Pt/X@MoO_3/C and Pt/C catalysts at temperatures below 40 °C. Thus, the mechanism for methanol oxidation reaction seems to be the same for all catalysts at 0.65 V and temperatures below 40 °C. Of course, the lower E_{ap} value observed for Pt/Mo_2C@MoO_3/C catalyst is associated with an increment of the catalytic activity due to the synergetic effect of the support. Furthermore, experiments (potentiodynamic and potentiostatic) suggest that the electrosorption and dehydrogenation step is governing the methanol oxidation rate at 0.65 V for all Pt/X@MoO_3/C catalysts in all temperature range studied. Analogous conclusions are derived from CO stripping experiments, in which the CO_{ad} oxidation reaction is considerably favoured at Pt/X@MoO_3/C catalysts (CO_{ad} can be removed from the catalyst surface at potentials as low as 0.1 V).

E_{ap} strongly depends on the specific catalytic reaction system. Parameters such as particle size, internal particle structure, applied potential, electrolyte and methanol concentration, counter ion, atomic surface arrangement and composition may lead to different values of E_{ap}. A wide range of E_{ap} values can be found in the literature for supported and unsupported Pt and PtRu (alloyed and not alloyed) varying from 42 to 100 kJ mol^{-1} [4,6,9,11]. However the lack of referenced E_{ap} values for systems similar to those in this paper, makes complicated, if not impossible, reliable comparison of our values with literature data. It is noteworthy the break to lower slopes at temperatures above 40 °C in Arrhenius plots. In fact, E_{ap} for Pt/Mo_2C@-MoO_3/C, Pt/Mo_{mix}@MoO_3/C and Pt/MoO_2@MoO_3/C at temperatures higher than 40 °C are 50%, 43% and 15.5% lower of those obtained at temperatures below 40 °C. The latter indicates that Pt/X@MoO_3/C materials suffer an internal diffusion limitation, which decreases as the MoO_2 content in the particle core increases [32]. This analysis is in agreement with the expected, since textural Mo_2C properties are similar to a metallic material without porosity, whereas MoO_2 presents the typical porosity degree of oxides. Consequently, besides the beneficial effect of the MoO_3 shell, the core nature of the support appears as the main important factor affecting the catalyst activity on this specific reaction, being the internal structure and electronic effect the best candidates to understand this influence.

On the other hand, E_{ap} for CO surface diffusion on Pt single-crystal and polycrystalline surfaces in the gas-phase revealed values between 16 and 29 kJ mol^{-1}, which is much lower values than the obtained for methanol oxidation [33–35]. In this context, it is noticeable the strong change in the E_{ap} for Pt/C at temperatures higher than 40 °C, being the value 16 kJ mol^{-1}, which is very close to the observed in gas phase for CO diffusion. Therefore, it is reasonably a modification of the mechanism governing the methanol oxidation rate on Pt/C catalyst at temperatures below/above 40 °C, that is from dissociative adsorption as the rds below 40 °C to electro-oxidation step (Eq. (6)) above 40 °C. Again, this in agreement with an external mass transfer limitation (lower methanol turnover rate due to adsorbed CO that blocks active sites) that predicts the two values of E_{ap}.

Summarizing, the same mechanism for methanol oxidation at 0.65 V on Pt/X@MoO_3/C in all temperature range studied and Pt/C at temperatures below 40 °C, which comprises the initial dissociative adsorption of methanol as rds. In addition, the applied potential of 0.65 V is enough to facilitate the methanolic residues (CO_{ad}) oxidation on Pt/X@MoO_3/C, and consequently a low CO_{ad} coverage is expected.

On the other hand, at temperatures higher than 40 °C, the dissociative adsorption of methanol increases on Pt/C catalyst, and consequently the CO_{ad} coverage rises. At this stage adsorbed methanolic fragments poison the Pt/C catalyst and its removal becomes the rds. Finally, methanol adsorption and dehydrogenation step governs the methanol oxidation rate for Pt/X@MoO_3/C catalysts in all whole temperature range studied. The main difference between Pt/X@MoO_3/C and Pt/C involves the higher catalytic activity towards CO_{ad} oxidation and stability during methanol oxidation provided by the X@MoO_3/C support. In this way, the CO removal is fast on Pt/X@MoO_3/C catalysts and the methanol dissociative adsorption controls the reaction rate.

5. Conclusion

Core–shell Mo-particles, with a reduced-Mo core (Mo_2C, MoO_2 and/or Mo^0) and a MoO_3-shell, were tested as Pt catalyst support for the CO and methanol oxidation reactions in the 20–70 °C temperature range. It was observed an important enhancement of the catalytic activity for both oxidation reactions when Mo_2C@-MoO_3/C was used as catalyst support. Remarkably, it is concluded that Mo-supports act only as promoter for these reactions. The improved tolerance towards CO was ascribed to a better dispersion of the active phase, to the facile oxygenated species formation on Pt/X@MoO_3/C catalysts (bi-functional mechanism) and to pure electronic effects (influence of the catalyst support on the electronic state of the active phase). In addition to these points, the performance towards methanol electro-oxidation was also influenced by the internal and external diffusion limitations of reactants and products, as well as to a strong electronic effect due to the core nature of the molybdenum based supports. Additionally, it is suggested the methanol dissociative adsorption as responsible for the methanol oxidation rate on Pt/X@MoO_3/C materials. Finally, Pt/X@MoO_3/C electrode containing only a Mo_2C phase in the core, develops the best performance (catalytic and stability) towards methanol oxidation along the time in all temperature range studied.

Acknowledgements

The authors wish to thank Spanish Ministry of Economy and Competitiveness (SMEC) for the financial support to project CTQ2011-28913-C02-02. RGL acknowledges the SMEC for her contract in the Project ENE2010-21198-C04-01. GG acknowledges to the JAE program (CSIC) for financial support. Also the use of General Research Services at the University of La Laguna (SEGAI-ULL) is acknowledged.

References

[1] A.S. Aricò, S. Srinivasan, V. Antonucci, Fuel Cells 1 (2001) 133–161.
[2] J. Kunze, U. Stimming, Angew. Chem. Int. Ed. 48 (2009) 9230–9237.
[3] H.A. Liebhafsky, E.J. Cairns, Fuel Cells and Fuel Batteries: A Guide to Their Research and Development, John Wiley and Sons, New York, 1969.
[4] W. Vielstich, Arnold Lamm, H.A. Gastaiger, Handbook of Fuel Cells: Fundamentals, Technology and Applications, John Wiley & Sons Ltd, Chichester, 2003.
[5] G. García, M.T.M. Koper, ChemPhysChem 12 (2011) 2064–2072.
[6] G. Garcia, V. Baglio, A. Stassi, E. Pastor, V. Antonucci, A. Aricò, J. Solid State Electrochem. 11 (2007) 1229–1238.
[7] G. García, J. Florez-Montaño, A. Hernandez-Creus, E. Pastor, G.A. Planes, J. Power Sources 196 (2011) 2979–2986.
[8] G.A. Planes, G. García, E. Pastor, Electrochem. Commun. 9 (2007) 839–844.
[9] N.M. Marković, P.N. Ross Jr., Surf. Sci. Rep. 45 (2002) 117–229.
[10] M.T.M. Koper, S.C.S. Lai, E. Herrero, in: M.T.M. Koper (Ed.), Fuel Cell Catalysis, a Surface Science Approach, Wiley, Hoboken, NJ, 2009, p. 159.
[11] M. Watanabe, H. Uchida, in: W. Vielstich, H. Yokokawa, H.A. Gastaiger (Eds.), Handbook of Fuel Cells: Fundamentals, Technology and Applications, John Wiley & Sons Ltd, Chichester, 2009, pp. 81–90.
[12] T. Iwasita, Electrochim. Acta 47 (2002) 3663–3674.
[13] E.A. Batista, G.R.P. Malpass, A.J. Motheo, T. Iwasita, Electrochem. Commun. 5 (2003) 843–846.
[14] A. Cuesta, J. Am. Chem. Soc. 128 (2006) 13332–13333.
[15] S. Gilman, J. Phys. Chem. 68 (1964) 70–80.
[16] A.S. Aricò, P.L. Antonucci, E. Modica, V. Baglio, H. Kim, V. Antonucci, Electrochim. Acta 47 (2002) 3723–3732.
[17] H.A. Gasteiger, N. Markovic, J.P.N. Ross, E.J. Cairns, J. Electrochem. Soc. 141 (1994) 1795–1803.
[18] L. Li, Y. Xing, Energies 2 (2009) 789–804.
[19] D. Ham, J. Lee, Energies 2 (2009) 873–899.
[20] R. Guil-López, M.V. Martínez-Huerta, O. Guillén-Villafuerte, M.A. Peña, J.L.G. Fierro, E. Pastor, Int. J. Hydrogen Energy 35 (2010) 7881–7888.
[21] O. Guillén-Villafuerte, R. Guil-López, E. Nieto, G. García, J.L. Rodríguez, E. Pastor, J.L.G. Fierro, Int. J. Hydrogen Energy 37 (2012) 7171–7179.
[22] M. Konsolakis, C. Drosou, I.V. Yentekakis, Appl. Catal. B Environ. 123–124 (2012) 405–413. and references there in.
[23] E.R. Gonzalez, E.A. Ticianelli, A.L.N. Pinheiro, J. Perez, in: INPI-SP No. 00321, 1997.
[24] Joint Committee on Powder Diffraction Standard, in: International Centre for Diffraction Data, Pennsylvania, 1997.
[25] O. Guillén-Villafuerte, G. García, A. Orive, B. Anula, A. Creus, E. Pastor, Electrocatalysis 2 (2011) 231–241.
[26] B. Geng, J. Cai, S. Liang, S.X. Liu, M.F. Li, Y.X. Chen, Phys. Chem. Chem. Phys. 12 (2010) 10888–10895.
[27] R. Gisbert, G. García, M.T.M. Koper, Electrochim. Acta 56 (2011) 2443–2449.
[28] M.T.M. Koper, Nanoscale 3 (2011) 2054–2073.
[29] N.P. Lebedeva, M.T.M. Koper, J.M. Feliu, R.A. van Santen, J. Electroanal. Chem. 524–525 (2002) 242–251.
[30] N.P. Lebedeva, M.T.M. Koper, J.M. Feliu, R.A. van Santen, J. Phys. Chem. B 106 (2002) 12938–12947.
[31] N.P. Lebedeva, M.T.M. Koper, E. Herrero, J.M. Feliu, R.A. van Santen, J. Electroanal. Chem. 487 (2000) 37–44.
[32] Françoise Duprat, Chem. Eng. Sci. 57 (2002) 901–911.
[33] M. Croci, C. Félix, G. Vandoni, W. Harbich, R. Monot, Surf. Sci. Lett. 290 (1993) L667–L672.
[34] B. Poelsema, L.K. Verheij, G. Comsa, Phys. Rev. Lett. 49 (1982) 1731–1735.
[35] J.E. Reutt-Robey, D.J. Doren, Y.J. Chabal, S.B. Christman, J. Chem. Phys. 93 (1990) 9113–9129.